

Bayesian inversion for electromyography using low-rank tensor formats

Anna Rörich* Tim A. Werthmann[†] Dominik Göttsche*[‡]
Lars Grasedyck[†]

September 8, 2020

Abstract

The reconstruction of the structure of biological tissue using electromyographic data is a non-invasive imaging method with diverse medical applications. Mathematically, this process is an inverse problem. Furthermore, electromyographic data are highly sensitive to changes in the electrical conductivity that describes the structure of the tissue. Modeling the inevitable measurement error as a stochastic quantity leads to a Bayesian approach. Solving the discretized Bayes-inverse problem means drawing samples from the posterior distribution of parameters, e.g., the conductivity, given measurement data. Using, e.g., a Metropolis-Hastings algorithm for this purpose involves solving the forward problem for different parameter combinations which requires a high computational effort. Low-rank tensor formats can reduce this effort by providing a data-sparse representation of all occurring linear systems of equations simultaneously and allow for their efficient solution. The application of Bayes' theorem proves the well-posedness of the Bayes-inverse problem. The derivation and proof of a low-rank representation of the forward problem allow for the precomputation of all solutions of this problem under certain assumptions, resulting in an efficient and theory-based sampling algorithm. Numerical experiments support the theoretical results, but also indicate that a high number of samples is needed to obtain reliable estimates for the parameters. The Metropolis-Hastings sampling algorithm, using the precomputed forward solution in a tensor format, draws this high number of samples and therefore enables solving problems which are infeasible using classical methods.

Keywords: inverse problem, parameter-dependent problem, Metropolis-Hastings algorithm, hierarchical Tucker format, EMG

*Institute of Applied Analysis and Numerical Simulation, University of Stuttgart, Allmandring 5b, 70569 Stuttgart, Germany

anna.roerich@ians.uni-stuttgart.de, dominik.goeddeke@ians.uni-stuttgart.de

[†]Institut für Geometrie und Praktische Mathematik, RWTH Aachen University, Templergraben 55, 52056 Aachen, Germany

werthmann@igpm.rwth-aachen.de, lgr@igpm.rwth-aachen.de

[‡]Stuttgart Center for Simulation Science, University of Stuttgart, Pfaffenwaldring 5a, 70569 Stuttgart, Germany

1 Introduction

In clinical applications, surface electromyographic (EMG) data are a widely used source of information about the muscular and nervous system. For example, EMG data are a valuable source of information in neurology, movement analysis, rehabilitation medicine or the development of biofeedback techniques. To this end, different models have been developed to simulate and understand EMG data, see, e.g., [25].

Using EMG measurements, we focus on reconstructing the intracellular conductivity of biological tissue. As the conductivity provides information about the structure of this tissue, we make an important step towards a non-invasive and radiation-free imaging method. Furthermore, reliable estimates on the conductivity from patient-specific EMG measurements can advance the personalized treatment.

Computed EMG data is, however, highly sensitive to changes in the conductivity, see, e.g., [20]. In addition, reconstructing data from (surface) measurements is an inverse problem [17]. Since the measurement error is unknown, we model it as a stochastic quantity and include it into the EMG model. This results in a probabilization of the whole EMG model. Consequently, the solution of the inverse EMG problem also becomes probabilistic.

For solving this probabilistic inverse problem, in Section 2, we use a Bayesian ansatz, cf. [5, 30], that searches for the probability distribution of the parameters for given measurements, the so-called *posterior distribution*. This ansatz has the advantage that the posterior distribution quantifies the uncertainty within instances of the reconstructed parameters.

Discretizing the posterior distribution means drawing a finite number of samples from the posterior which includes solving the (discrete) forward EMG problem for different parameter samples to check the fidelity of each sample.

As solving the forward EMG problem is expensive using classical methods, we aim at precomputing the solution of the forward problem for all parameters at the same time. This results in a parameter-dependent linear system of equations, i.e., $A(p)\phi(p) = b(p)$ for an operator A , a solution ϕ , and a right-hand side b depending on parameters $p = (p^{(1)}, p^{(2)}, \dots, p^{(d)})$. After discretizing the parameters in the sense that we allow each parameter $p^{(j)}$, $j = 1, \dots, d$, to take n different values from its domain, solving the linear system for every combination of parameters implies solving n^d linear systems. This exponential scaling in the dimension d of the parameter space is commonly known as the *curse of dimensionality* which renders classical methods for $d \gg 2$ infeasible.

To represent these parameter-dependent linear systems, we use low-rank tensor formats, cf. [12, 14], which we recapitulate in Section 3. Solving these linear systems within these formats allows us to evaluate the parameter-dependent forward problem fast.

In particular, our main contributions to solve this Bayes-inverse EMG problem and to represent the forward problem in a data-sparse way using low-rank tensor formats are:

- We prove the well-posedness of our particular Bayes-inverse EMG problem in Section 4 and show that modeling the measurement error leads to a natural regularization of the inverse problem.

- We derive a discretization of the parameter-dependent operator and the right-hand side in Section 5 and prove a data-sparse representation of this discretization using low-rank tensor formats. This method allows us to solve the parameter-dependent linear system fast.
- Combining this data-sparse representation with a standard Metropolis-Hastings algorithm in Section 6 allows us to solve the Bayes-inverse EMG problem efficiently.

In Section 7, we present our numerical experiments that support our theoretical analysis and indicate that the Markov chain constructed by the Metropolis-Hastings algorithm using low-rank tensor formats behaves like the Markov chain constructed by a standard algorithm. Further, we observe a speedup of more than 600 using low-rank tensor formats compared to a standard algorithm.

In Section 8, we discuss some related work, and in Section 9, we conclude that mathematical theory and an efficient representation of the parameter-dependent solution, which allows us to generate samples fast, leads to an efficient algorithm to solve the Bayes-inverse problem.

2 The Bayes-inverse electromyographic problem

In order to define our Bayes-inverse EMG problem, we briefly discuss the structure of skeletal muscles and summarize a forward model of surface EMG signals in the following.

A skeletal muscle is composed of bundles of cells, the so-called muscle fibers. These muscle fibers are the active contractile tissue of a body that react to electrical stimuli. Neglecting the presence of bones, a skeletal muscle is surrounded and protected by a layer of connective tissue, fat and skin.

Surface EMG signals are electrical signals that are measured at the skin surface. To model surface EMG signals, we follow the physical structure of a skeletal muscle beginning with the electrical behavior of a single muscle fiber, then describing the electrical behavior of a skeletal muscle by assembling the muscle fibers, and finally modeling the propagation of an electrical signal through the surrounding tissue.

An electrical stimulus from the spinal cord influences the chemo-electrical behavior of the innervated muscle fibers $D_{F,j} \subseteq \mathbb{R}$, $j = 1, \dots, N_{MF}$, for $N_{MF} \in \mathbb{N}$ muscle fibers. These electrical fluctuations travel along the muscle fibers as action potentials (APs), propagate through the muscle and subcutaneous tissue, and are measured at $M \in \mathbb{N}$ measuring points summarized in $\mathbf{x} \in \mathbb{R}^{M \times 3}$.

We apply the widely used model by Rosenfalck [27] to model the muscle fiber AP:

$$v_{m,j}(s) = r_{1,j}s^3 \exp(-r_{2,j}s) - r_{3,j} \quad \text{for } s \in D_{F,j}, j = 1, \dots, N_{MF}. \quad (1)$$

Here, $r_{1,j}, r_{2,j}, r_{3,j} \in \mathbb{R}$ are known, fixed constants, and the spatial coordinate s can be rewritten as $s = u_j t$ using the AP velocities u_j and time t .

To assemble a three-dimensional skeletal muscle $D_M \subseteq \mathbb{R}^3$ from the one-dimensional muscle fibers $D_{F,j} \subseteq \mathbb{R}$, a transfer operator is needed. Thus, we introduce the smoothing

operator $S : D_{F,j} \rightarrow \mathbb{R}^3$ with

$$S(v_{m,j})(x) = v_{m,j}(\pi_j(x)) \exp\left(-\frac{\beta}{2} \|x - \pi_j(x)\|_{\mathbb{R}^3}^2\right), \quad (2)$$

where $\beta \in \mathbb{R}$ is a smoothing parameter and $\pi_j : D_M \rightarrow D_{F,j}$ is the orthogonal projection of a muscle tissue point $x \in D_M$ onto the muscle fiber $D_{F,j}$ with starting point $y_j \in \mathbb{R}^3$ and direction $\vec{d}_j \in \mathbb{R}^3$. Note that the muscle fiber directions \vec{d}_j in general depend on $x \in \mathbb{R}^3$ and are known for the forward problem, e.g., through a medical imaging technique. The projection reads

$$\pi_j(x) = y_j + \frac{(x - y_j)^\top \vec{d}_j}{\vec{d}_j^\top \vec{d}_j} \vec{d}_j. \quad (3)$$

Applying the smoothing operator to the muscle fibers yields $\cup_{j=1}^{N_{MF}} S(D_{F,j}) = D_M$, and we obtain the membrane potential $V_m(x) = \sum_{j=1}^{N_{MF}} S(v_{m,j})(x)$.

The bidomain equation, as stated in [25], models the propagation of the membrane potential V_m through a skeletal muscle by

$$\nabla \cdot ((\sigma_i + \sigma_e) \nabla \phi_e) = -\nabla \cdot (\sigma_i \nabla V_m) \quad \text{in } D_M,$$

where ϕ_e denotes the extracellular electrical potential, and σ_i , σ_e are the intra- and extracellular electrical conductivities.

Note that we model the conductivities as matrix-valued functions, e.g., $\sigma_i(x) \in \mathbb{R}^{3 \times 3}$ for all $x := (x_1, x_2, x_3)^\top \in D_M$, where each matrix entry $(\sigma_i)_{j,k}$ quantifies the conductivity of the tissue in the x_j - x_k -direction for $j, k = 1, 2, 3$. In particular, the eigenvector of $\sigma_i(x)$ that belongs to the largest eigenvalue represents the orientation of the underlying muscle fiber, and the largest eigenvalue corresponds to the longitudinal conductivity of the underlying muscle fiber. This relation enables us to draw conclusions about the structure of muscular tissue from its intracellular conductivity.

Leaving the muscle tissue, the subsequent propagation of the electrical potential through the surrounding tissue $D_B \subseteq \mathbb{R}^3$ is described by

$$\nabla \cdot (\sigma_0 \nabla \phi_0) = 0 \quad \text{in } D_B. \quad (4)$$

Here, $\sigma_0 \in \mathbb{R}^{3 \times 3}$ is the electrical conductivity of the surrounding tissue and ϕ_0 its electrical potential.

For ensuring smoothness of the electrical potentials across the tissue boundary, the authors in [25] postulate the following coupling conditions:

$$\begin{aligned} \phi_e &= \phi_0 && \text{on } \Gamma_I, \\ (\sigma_e \nabla \phi_e) \cdot \vec{n}_M &= -(\sigma_0 \nabla \phi_0) \cdot \vec{n}_B && \text{on } \Gamma_I. \end{aligned}$$

Here, $\vec{n}_{(\cdot)}$ denotes the outer normal vector of the indexed domain and $\Gamma_I := \partial D_M \cap \partial D_B$ denotes the interface between muscle tissue and subcutaneous tissue. Additionally, no-

flow boundary conditions are introduced at all outer domain boundaries

$$\begin{aligned} (\sigma_i \nabla V_m) \cdot \vec{n}_M &= -(\sigma_i \nabla \phi_e) \cdot \vec{n}_M && \text{on } \partial D_M, \\ (\sigma_0 \nabla \phi_0) \cdot \vec{n}_B &= 0 && \text{on } \Gamma_B, \\ (\sigma_e \nabla \phi_e) \cdot \vec{n}_M &= 0 && \text{on } \Gamma_M, \end{aligned}$$

where $\Gamma_B := \partial D_B \setminus \Gamma_I$ is the outer body boundary, and $\Gamma_M := \partial D_M \setminus \Gamma_I$ is the outer muscle boundary. A zero-mean integral condition is used to achieve a unique solution:

$$\int_{D_M} \phi_e + \int_{D_B} \phi_0 = 0. \quad (5)$$

Further, the abbreviations $D := D_M \cup D_B$ and

$$\phi(x) := \begin{cases} \phi_e(x) & \text{for } x \in D_M, \\ \phi_0(x) & \text{for } x \in D_B \end{cases}$$

are used such that (5) reads $\int_D \phi = 0$.

We refer to [25] and the references therein for a model of force generation and the corresponding continuum mechanics. Within our setting, the muscle geometry and the structure of the tissue remain unchanged in time.

A reasonable assumption on σ_i is that it is bounded, i.e., there exist constants $s_- > 0$ and $s_+ < \infty$ such that $s_- \leq \sigma_i(x) \leq s_+$ holds for all $x \in D_M$. Physically this corresponds to the tissue neither being fully insulating nor super conducting. Formalizing these considerations leads to the assumption $\sigma_i \in L^\infty(D, \mathbb{R}^{3 \times 3})$, where we set $\sigma_i = 0$ in D_B .

For simplicity, we encapsulate the above models in the definition of the observation operator

$$\mathcal{G}_x : L^\infty(D, \mathbb{R}^{3 \times 3}) \rightarrow \mathbb{R}^M \quad \text{with } \sigma_i \mapsto \phi(\mathbf{x}), \quad (6)$$

which maps a given intracellular conductivity σ_i to the calculated electrical potential $\phi(\mathbf{x})$ at measuring points $\mathbf{x} \in \mathbb{R}^{M \times 3}$.

To complete the forward EMG model, we include the inevitable measurement error which is unknown but is usually assumed to be additive and to follow a normal distribution. Hence, the measurement error is modeled as a random variable $\eta : \Omega \rightarrow \mathbb{R}^M$ on a complete probability space (Ω, \mathcal{F}, P) with $\eta \sim \mathcal{N}(0, \Xi)$ and covariance matrix $\Xi = \text{diag}(\xi, \dots, \xi) \in \mathbb{R}^{M \times M}$. Adding the measurement error to (6) yields the model for EMG data

$$\phi_{\text{EMG}}^{\text{comp}}(\sigma_i) = \phi_{\text{EMG}}^{\text{comp}}(\sigma_i, \mathbf{x}, \omega) := \mathcal{G}_x(\sigma_i) + \eta(\omega) \in \mathbb{R}^M. \quad (7)$$

Solving (7) for σ_i , as in the inverse problem setting, shows that σ_i must be a random variable as well. For emphasizing the randomness of σ_i , we write $\sigma_i = \sigma_i(x, \omega)$ and assume that $\sigma_i \in L^q(\Omega; L^\infty(D, \mathbb{R}^{3 \times 3}))$ for some $q \geq 2$ with $L^q(\Omega; L^\infty(D, \mathbb{R}^{3 \times 3}))$ denoting a Lebesgue-Bochner space. From this assumption we deduce that the Karhunen-Loève expansion

$$\sigma_i(x, \omega) = \bar{\sigma}(x) + \sum_{j \geq 1} T_j(\omega) \psi_j(x) \quad (8)$$

exists with $\bar{\sigma}(x) \in L^\infty(D, \mathbb{R}^{3 \times 3})$ denoting the mean of $\sigma_i(x, \omega)$ and random coefficients $T_j : \Omega \rightarrow [-1, 1]$, cf., e.g., [1]. Thus, searching for σ_i is equivalent to finding realizations $(T_j(\omega))_{j \geq 1} \in [-1, 1]^{\mathbb{N}} =: \mathcal{J}$ when we fix a suitable basis $(\psi_j)_{j \geq 1}$ of $L^\infty(D, \mathbb{R}^{3 \times 3})$. As done in [19], we make the following assumption to guarantee the convergence of (8).

Assumption 2.1. There exists a constant $0 < \kappa < \infty$ such that $\sum_{j \geq 1} \|\psi_j\|_{L^\infty} \leq \kappa$ holds.

Note that this assumption implies the (almost sure) boundedness of the conductivity, by some parameters s_- and s_+ , as discussed above and is thus physically reasonable.

A naive inversion of the probabilistic forward problem would be to search for a $\sigma_i(\omega) \in L^\infty(D, \mathbb{R}^{3 \times 3})$ such that $\phi_{\text{EMG}}^{\text{comp}}(\sigma_i(\omega)) = \phi_{\text{EMG}}^{\text{meas}}$ for given measurements $\phi_{\text{EMG}}^{\text{meas}} \in \mathbb{R}^M$. This problem formulation searches for particular realizations of the random variable σ_i that, however, misrepresents the behavior of the probabilistic inverse EMG problem. Hence, we need a more appropriate problem formulation.

We consider a function space Bayesian formulation which aims at calculating the probability distribution of σ_i for given data $\phi_{\text{EMG}}^{\text{meas}}$.

To follow this approach, we equip \mathcal{J} with the product σ -algebra Θ , with $\Theta := \otimes_{j \geq 1} \mathcal{B}([-1, 1])$, where $\mathcal{B}([-1, 1])$ is the Borel- σ -algebra on $[-1, 1]$. Subsequently, the product probability measure $\rho := \otimes_{j \geq 1} d\lambda_j$ is defined on the measurable space (\mathcal{J}, Θ) with $d\lambda_j$ denoting the normalized product Lebesgue measure on $[-1, 1]$, similar to [19, 28]. Note that ρ is the probability law of the random variable $T := (T_j)_{j \geq 1}$, since the T_j are uncorrelated and uniformly distributed. In the Bayesian context, ρ is called the *prior measure* or short *prior*, because it describes the behavior of T prior to having any knowledge about the conductivity, e.g., from measurements.

The Bayes-inverse EMG problem searches for the conditioned probability distribution ρ^{EMG} of σ_i given EMG measurements $\phi_{\text{EMG}}^{\text{meas}}$. We prove the existence of the posterior distribution ρ^{EMG} in Section 4.

For solving our Bayes-inverse EMG problem, we use a Metropolis-Hastings algorithm, see, e.g., [26]. A Metropolis-Hastings algorithm is an acceptance-rejection algorithm that draws samples from the posterior distribution by solving the EMG forward problem for different realizations of T , i.e., of σ_i and comparing the results. If the proposal is accepted by an acceptance strategy a , it becomes part of a Markov chain. Otherwise, the old sample will be kept and a new proposal will be drawn as shown in Algorithm 1.

In [5], the acceptance strategy $a(T^{(j)}, \tilde{T}) := \min\{1, \exp(\Phi(T^{(j)}) - \Phi(\tilde{T}))\}$ with the potential $\Phi : \mathcal{J} \times \mathbb{R}^M \rightarrow \mathbb{R}$ defined by

$$\Phi(T, \phi_{\text{EMG}}^{\text{meas}}) := \frac{1}{2} \|\phi_{\text{EMG}}^{\text{meas}} - \mathcal{G}_{\mathbf{x}}(T)\|_{\Xi}^2 - \frac{1}{2} \|\phi_{\text{EMG}}^{\text{meas}}\|_{\Xi}^2 \quad (9)$$

and Ξ -norm $\|\mathbf{v}\|_{\Xi} := \left\| \Xi^{-\frac{1}{2}} \mathbf{v} \right\|_{\mathbb{R}^M}$ for all $\mathbf{v} \in \mathbb{R}^M$ was derived such that the resulting Markov chain is reversible with respect to the prior ρ . This yields the convergence of Algorithm 1.

Algorithm 1 Metropolis-Hastings.

Input: Starting point $T^{(1)}$ for the Markov chain

Output: A Markov chain T

```
1: for  $j \geq 1$  do
2:   Propose  $\tilde{T} \sim \rho$  independent of  $T^{(j)}$ 
3:   Draw  $c \sim \mathcal{U}(0, 1)$ 
4:   if  $c \leq a(T^{(j)}, \tilde{T})$  then
5:      $T^{(j+1)} = \tilde{T}$ 
6:   else
7:      $T^{(j+1)} = T^{(j)}$ 
8:   end if
9: end for
```

We rewrite the acceptance strategy neglecting the iteration index for the samples $T^{(j)}$:

$$\begin{aligned} a(T, \tilde{T}) &= \min \{1, \exp(\Phi(T) - \Phi(\tilde{T}))\} \\ &= \min \left\{ 1, \frac{\exp\left(\frac{1}{2} \|\phi_{\text{EMG}}^{\text{meas}} - \mathcal{G}_{\mathbf{x}}(T)\|_{\Xi}^2\right)}{\exp\left(\frac{1}{2} \|\phi_{\text{EMG}}^{\text{meas}} - \mathcal{G}_{\mathbf{x}}(\tilde{T})\|_{\Xi}^2\right)} \right\} \\ &\begin{cases} = 1 & \text{if } \|\phi_{\text{EMG}}^{\text{meas}} - \mathcal{G}_{\mathbf{x}}(\tilde{T})\|_{\Xi}^2 \leq \|\phi_{\text{EMG}}^{\text{meas}} - \mathcal{G}_{\mathbf{x}}(T)\|_{\Xi}^2, \\ < 1 & \text{otherwise.} \end{cases} \end{aligned}$$

Consequently, a new proposal will always be accepted, if it produces a smaller error than the last accepted sample, and will otherwise be rejected with probability $1 - a$, i.e., the old sample will be kept with probability $1 - a$.

3 Low-rank tensor formats

Evaluating the acceptance strategy in every step of the Metropolis-Hastings algorithm requires the evaluation of the observation operator $\mathcal{G}_{\mathbf{x}}$, i.e., the solution of the forward EMG problem, for a new intracellular conductivity $\sigma_i = \bar{\sigma}(x) + \sum_{j \geq 1} T_j(\omega) \psi_j(x)$. Consequently, we need a way to compute these solutions fast. We use low-rank tensor formats to accelerate these computations and motivate these formats using an example, analog to [11].

We consider the scaling of a discrete operator A_{h} by a parameter $p_{\text{h}}(j)$, $j = 1, \dots, n$ with $n \in \mathbb{N}$, i.e., $p_{\text{h}}(j)A_{\text{h}}$. We assume that the right-hand side b_{h} is constant for all $p_{\text{h}}(j)$. Using classical methods, we would need to solve the following linear system:

$$\begin{pmatrix} p_{\text{h}}(1)A_{\text{h}} & 0 & \dots & 0 \\ 0 & p_{\text{h}}(2)A_{\text{h}} & \ddots & \vdots \\ \vdots & \ddots & \ddots & 0 \\ 0 & \dots & 0 & p_{\text{h}}(n)A_{\text{h}} \end{pmatrix} \begin{pmatrix} \phi_{\text{h}}(p_{\text{h}}(1)) \\ \phi_{\text{h}}(p_{\text{h}}(2)) \\ \vdots \\ \phi_{\text{h}}(p_{\text{h}}(n)) \end{pmatrix} = \begin{pmatrix} b_{\text{h}} \\ b_{\text{h}} \\ \vdots \\ b_{\text{h}} \end{pmatrix}.$$

Using the Kronecker product to reformulate this system

$$(\text{diag}(p_h(1), p_h(2), \dots, p_h(n)) \otimes A_h) \phi_h(p_h) = (1, \dots, 1)^\top \otimes b_h,$$

we achieve a data-sparse representation. We use a generalization of this representation to derive a data-sparse representation of the parameter-dependent forward EMG problem which can be interpreted as the *CANDECOMP/PARAFAC*, or short *CP, representation* introduced in [3, 18].

Definition 3.1 (CP representation and CP decomposition). A *CP representation* of a tensor $\mathbf{B} \in \mathbb{R}^{\mathcal{I}}$, with *representation rank* $r \in \mathbb{N}_0$, is defined as

$$\mathbf{B} = \sum_{k=1}^r \bigotimes_{\ell=1}^d b_k^{(\ell)} \quad \text{with } b_k^{(\ell)} \in \mathbb{R}^{\mathcal{I}_\ell}, \quad (10)$$

where $\mathcal{I} = \times_{\ell=1}^d \mathcal{I}_\ell$ is an index set with $|\mathcal{I}_\ell| = n_\ell$ for all $\ell \in \mathcal{D} := \{1, \dots, d\}$. We call each $\ell \in \mathcal{D}$ *mode* and d the *dimension*. The minimal r , such that (10) holds, is called the *CP rank* of \mathbf{B} and in this case (10) is called the *CP decomposition* of \mathbf{B} . Tensors of the form $\bigotimes_{\ell=1}^d b^{(\ell)}$, i.e., tensors of rank 1, are called *elementary tensors*.

A big advantage of the CP format is the data-sparsity in case of a small representation rank r , since a tensor $\mathbf{B} \in \mathbb{R}^{\mathcal{I}}$ of the form (10) has storage cost in $\mathcal{O}(r \sum_{\ell=1}^d |\mathcal{I}_\ell|) \approx \mathcal{O}(rdn)$ compared to $\mathcal{O}(\prod_{\ell=1}^d |\mathcal{I}_\ell|) \approx \mathcal{O}(n^d)$ with $n = \max_{\ell \in \mathcal{D}} n_\ell$.

Therefore it is desirable to represent the operator and the right-hand side of the forward EMG problem data-sparse using low-rank tensor formats. To compute the solution of the discrete forward EMG problem, we need to solve linear systems within low-rank tensor formats. An algorithm that can calculate the inverse of an operator with rank $r > 1$ in a direct way is unknown.

Consider, e.g., a CP operator \mathbf{A} of dimension 1 and rank 2, i.e., $\mathbf{A} = A_1 + A_2$, with $A_1, A_2 \in \mathbb{R}^{n \times n}$. Then, finding a direct inverse of \mathbf{A} in the CP format means finding matrices C_j and D_j such that $\mathbf{A}^{-1} = (A_1 + A_2)^{-1} \stackrel{!}{\approx} \sum_{j=1}^J C_j^{-1} + D_j^{-1}$ holds for some rank $J \in \mathbb{N}$. Since such a property is unknown even for matrix summations [24], it is also unknown in the more general tensor case.

We therefore need iterative solvers and thus arithmetic operations within low-rank tensor formats. These arithmetic operations often lead to an increase of the representation rank.

Consider, e.g., a CP operator of dimension 2 and rank 3, i.e., $\mathbf{A} = \sum_{i=1}^3 A_i^{(1)} \otimes A_i^{(2)}$ and a CP vector of dimension 2 and rank 2, i.e., $\mathbf{x} = \sum_{j=1}^2 x_j^{(1)} \otimes x_j^{(2)}$. Then, the application of \mathbf{A} to \mathbf{x} yields $\mathbf{A}\mathbf{x} = (\sum_{i=1}^3 A_i^{(1)} \otimes A_i^{(2)}) (\sum_{j=1}^2 x_j^{(1)} \otimes x_j^{(2)}) = \sum_{i=1}^3 \sum_{j=1}^2 A_i^{(1)} x_j^{(1)} \otimes A_i^{(2)} x_j^{(2)} = \sum_{k=1}^6 y_k^{(1)} \otimes y_k^{(2)}$ with $y_k^{(\nu)} := A_i^{(\nu)} x_j^{(\nu)}$ for $k = i + 3(j - 1)$ and $\nu = 1, 2$. Therefore $\mathbf{A}\mathbf{x}$ is a CP vector of representation rank 6 ($= 2 \cdot 3$).

The above example shows that we need a truncation of a tensor to lower rank, i.e., an approximation with a tensor of lower rank. To guarantee the convergence of iterative methods, we have to guarantee that the truncation error is small enough, cf. [15].

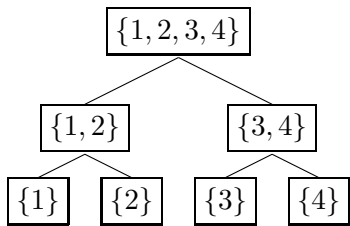


Figure 1: Dimension tree for dimension $d = 4$.

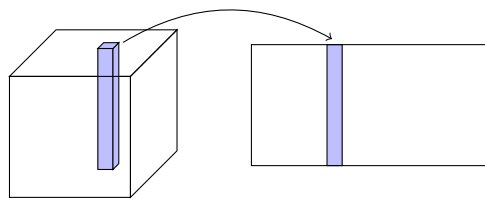


Figure 2: Visual representation of a matricization.

The set of CP tensors of rank r is, however, not closed which makes the approximation of a CP tensor of rank r an ill-posed problem, cf. [29]. Therefore, we cannot guarantee that the truncation error will be small enough to yield convergence of the iterative method. To overcome this drawback, we use the *hierarchical Tucker* format to represent and compute the solution of a linear system.

The general idea of the hierarchical Tucker format, which was first introduced in [16] and further analyzed in [10], is to define a hierarchy among the modes $\mathcal{D} = \{1, \dots, d\}$. To do so, we define the so-called *dimension tree* \mathcal{T} analogously to [10, Definition 3.1].

Definition 3.2 (dimension tree). A *dimension tree* \mathcal{T} for dimension $d \in \mathbb{N}$ is a binary tree with nodes labeled by non-empty subsets of \mathcal{D} . Its root is labeled with \mathcal{D} and each node $w \in \mathcal{T}$ satisfies exactly one of the following possibilities:

- (i) w is a leaf of \mathcal{T} and is labeled with a single-element subset $z = \{\ell\} \subseteq \mathcal{D}$. The set of all leaves is called $\mathcal{L}(\mathcal{T})$.
- (ii) $w \in \mathcal{I}(\mathcal{T}) := \mathcal{T} \setminus \mathcal{L}(\mathcal{T})$ is an inner node of \mathcal{T} and has exactly two children $w_1, w_2 \in \mathcal{T}$, for which the corresponding labels $z, z_1, z_2 \subseteq \mathcal{D}$ with $z, z_1, z_2 \neq \emptyset$ fulfill $z = z_1 \dot{\cup} z_2$.

We will identify a node w with its label z and therefore also write $z \in \mathcal{T}$.

Figure 1 shows an example of a dimension tree for $d = 4$. Each node $w \in \mathcal{T}$ represents a non-empty subset $z \subseteq \mathcal{D}$ of the modes. This leads to the corresponding *matricization* for each node which we define as in [10, Definition 3.3]:

Definition 3.3 (matricization and vectorization). Let $\mathbf{B} \in \mathbb{R}^{\mathcal{I}}$, $z \subseteq \mathcal{D}$ with $z \neq \emptyset$, and $g := \mathcal{D} \setminus z$. The *matricization* of \mathbf{B} corresponding to z is defined as $\mathbf{B}^{(z)} \in \mathbb{R}^{\mathcal{I}_z \times \mathcal{I}_g}$, where $\mathcal{I}_z := \times_{\ell \in z} \mathcal{I}_\ell$ and $\mathcal{I}_g := \times_{\ell \in g} \mathcal{I}_\ell$, with $\mathbf{B}^{(z)}[(i_j)_{j \in z}, (i_j)_{j \in g}] := \mathbf{B}[i_1, \dots, i_d]$ for all $i = (i_j)_{j \in \mathcal{D}}$. In particular, $\mathbf{B}^{(\mathcal{D})} \in \mathbb{R}^{\mathcal{I}}$ holds, which can also be interpreted as the *vectorization* of \mathbf{B} .

A matricization can be interpreted as an unfolding of the tensor as illustrated in Figure 2. Based on the concept of matricizations the *hierarchical Tucker rank* is defined accordingly to [10, Definition 3.4]:

Definition 3.4 (hierarchical Tucker rank). Let $\mathbf{B} \in \mathbb{R}^{\mathcal{I}}$ and \mathcal{T} be a dimension tree. The *hierarchical Tucker rank* of \mathbf{B} is defined as $\text{rank}_{\mathcal{T}}(\mathbf{B}) := (r_z)_{z \in \mathcal{T}}$, where $r_z := \text{rank}(\mathbf{B}^{(z)})$ denotes the matrix rank of the matricization $\mathbf{B}^{(z)}$ for all $z \in \mathcal{T}$.

The set of tensors with hierarchical Tucker rank node-wise bounded by $(r_z)_{z \in \mathcal{T}}$ is defined as $\mathcal{H}\text{-Tucker}(\mathcal{T}, (r_z)_{z \in \mathcal{T}}) := \{\mathbf{C} \in \mathbb{R}^{\mathcal{I}} \mid \text{rank}(\mathbf{C}^{(z)}) \leq r_z \text{ for all } z \in \mathcal{T}\}$.

By construction the so-called *nestedness property*

$$\begin{aligned} \text{span}\{\mathbf{B}^{(z)}[\cdot, i] \mid 1 \leq i \leq r_z\} \subseteq \\ \text{span}\{\mathbf{B}^{(z_1)}[\cdot, i_1] \otimes \mathbf{B}^{(z_2)}[\cdot, i_2] \mid 1 \leq i_j \leq r_{z_j}, j = 1, 2\} \end{aligned} \quad (11)$$

holds for all $z \in \mathcal{I}(\mathcal{T})$ with children $z_1, z_2 \in \mathcal{T}$. The nestedness property (11) allows us to represent the tensor in an efficient way, similarly to [10, Definition 3.5].

Definition 3.5 ((nested) generator and transfer tensor). Let $\mathbf{B} \in \mathbb{R}^{\mathcal{I}}$, \mathcal{T} be a dimension tree and $r_z \in \mathbb{N}$ for all $z \in \mathcal{T}$. A family of matrices $(U_z)_{z \in \mathcal{T}}$, also called a *frame tree*, with frames $U_z = (U_z[\cdot, 1] \mid \dots \mid U_z[\cdot, r_z]) \in \mathbb{R}^{\mathcal{I}_z \times r_z}$ is called a *generator* of \mathbf{B} , if $\text{range}(\mathbf{B}^{(z)}) \subseteq \text{range}(U_z)$ holds for all $z \in \mathcal{T}$.

The frame tree $(U_z)_{z \in \mathcal{T}}$ is called *nested*, if for all $z \in \mathcal{I}(\mathcal{T})$ with children $z = \{z_1, z_2\}$ it holds $U_z[\cdot, i] \in \text{span}\{U_{z_1}[\cdot, i_1] \otimes U_{z_2}[\cdot, i_2] \mid 1 \leq i_j \leq r_{z_j}, j = 1, 2\}$ for all $i \in \{1, \dots, r_z\}$.

Let further U_g be a matrix which contains column by column a basis of $\text{range}(\mathbf{B}^{(g)})$ for $g \in \{z, z_1, z_2\}$. Then there exist coefficients $B_z[i, i_1, i_2] \in \mathbb{R}$ such that $U_z[\cdot, i] = \sum_{i_1=1}^{r_{z_1}} \sum_{i_2=1}^{r_{z_2}} B_z[i, i_1, i_2] (U_{z_1}[\cdot, i_1] \otimes U_{z_2}[\cdot, i_2])$ holds. The corresponding tensor $B_z \in \mathbb{R}^{r_z \times r_{z_1} \times r_{z_2}}$ is called *transfer tensor*.

We represent \mathbf{B} , using the nestedness property (11), by providing the transfer tensors B_z for all $z \in \mathcal{I}(\mathcal{T})$ and the frames U_z for all $z \in \mathcal{L}(\mathcal{T})$. For computing the matrices U_z for $z \in \mathcal{T}$, e.g., the singular value decomposition can be applied to the corresponding matricizations $\mathbf{B}^{(z)}$. Assuming that the frames U_g with $g \in \{z, z_1, z_2\}$ contain orthonormal bases of the range of the corresponding matricizations, the transfer tensor is given by $B_z[i, i_1, i_2] = \langle U_z[\cdot, i], U_{z_1}[\cdot, i_1] \otimes U_{z_2}[\cdot, i_2] \rangle$, where $\langle \cdot, \cdot \rangle$ denotes the Euclidean scalar product. We now define the *hierarchical Tucker format representation* of a tensor as in [10, Definition 3.6].

Definition 3.6 (hierarchical Tucker format). Let $\mathbf{B} \in \mathbb{R}^{\mathcal{I}}$, \mathcal{T} be a dimension tree, $r_z \in \mathbb{N}$ for all $z \in \mathcal{T}$ with $r_{\mathcal{D}} = 1$, $(U_z)_{z \in \mathcal{L}(\mathcal{T})}$ a nested generator of \mathbf{B} with $U_z \in \mathbb{R}^{\mathcal{I}_z \times r_z}$, and $(B_z)_{z \in \mathcal{I}(\mathcal{T})}$ the corresponding transfer tensors. Then we call $((U_z)_{z \in \mathcal{L}(\mathcal{T})}, (B_z)_{z \in \mathcal{I}(\mathcal{T})})$ a *hierarchical Tucker representation* of \mathbf{B} . The vector $(r_z)_{z \in \mathcal{T}}$ is called *representation rank*.

The memory required for a hierarchical Tucker representation, with dimension tree \mathcal{T} and representation rank $(r_z)_{z \in \mathcal{T}}$, of a tensor $\mathbf{B} \in \mathbb{R}^{\mathcal{I}}$ for $n = \max_{\ell \in \mathcal{D}} n_{\ell}$ and $r = \max_{z \in \mathcal{T}} r_z$ is given by $\mathcal{O}(rdn + r^3d)$, cf. [10, Lemma 3.7]. The existence of a truncation method of a low-rank tensor $\mathbf{B} \in \mathcal{H}\text{-Tucker}(\mathcal{T}, (r_z)_{z \in \mathcal{T}})$ down to lower rank $(\tilde{r}_z)_{z \in \mathcal{T}}$ with an arithmetic cost in $\mathcal{O}(r^2dn + r^4d)$ was proven in [10]. The resulting approximation $\tilde{\mathbf{B}} := \text{truncate}(\mathbf{B}) \in \mathcal{H}\text{-Tucker}(\mathcal{T}, (\tilde{r}_z)_{z \in \mathcal{T}})$ fulfills the quasi-optimal error estimation

$$\|\mathbf{B} - \tilde{\mathbf{B}}\| \leq \sqrt{2d-3} \inf_{\mathbf{C} \in \mathcal{H}\text{-Tucker}(\mathcal{T}, (\tilde{r}_z)_{z \in \mathcal{T}})} \|\mathbf{B} - \mathbf{C}\|.$$

Further, we can transfer a CP representation of a tensor with CP rank r into a hierarchical Tucker representation with rank node-wise bounded by r , cf. [14, Theorem 11.17]. Following this approach, we represent the operator and the right-hand side in the hierarchical Tucker format. For solving parameter-dependent linear problems in the hierarchical Tucker format, we use the preconditioned conjugate gradients (PCG) method. In Algorithm 2 the PCG method is briefly introduced similar to [22, Algorithm 2].

Algorithm 2 preconditioned conjugate gradients method with truncation.

Input: Operator \mathbf{A} , right-hand side \mathbf{b} , CP rank 1 preconditioner \mathbf{M} , initial guess $\phi^{(0)}$ in the hierarchical Tucker format

Output: Approximate solution ϕ in the hierarchical Tucker format of $\mathbf{A}\phi = \mathbf{b}$

- 1: $\mathbf{R}^{(0)} = \text{truncate}(\mathbf{b} - \mathbf{A}\phi^{(0)})$
 - 2: $\mathbf{Z}^{(0)} = \mathbf{M}^{-1}\mathbf{R}^{(0)}$
 - 3: $\mathbf{P}^{(0)} = \mathbf{Z}^{(0)}$
 - 4: $\mathbf{Q}^{(0)} = \text{truncate}(\mathbf{A}\mathbf{P}^{(0)})$
 - 5: $k = 0$
 - 6: **while** $\frac{\|\mathbf{R}^{(k)}\|}{\|\mathbf{b}\|} > \varepsilon$ **and** $k < k_{\max}$ **do**
 - 7: $\phi^{(k+1)} = \text{truncate}\left(\phi^{(k)} + \frac{\langle \mathbf{R}^{(k)}, \mathbf{P}^{(k)} \rangle}{\langle \mathbf{Q}^{(k)}, \mathbf{P}^{(k)} \rangle} \mathbf{P}^{(k)}\right)$
 - 8: $\mathbf{R}^{(k+1)} = \text{truncate}(\mathbf{b} - \mathbf{A}\phi^{(k+1)})$
 - 9: $\mathbf{Z}^{(k+1)} = \mathbf{M}^{-1}\mathbf{R}^{(k+1)}$
 - 10: $\mathbf{P}^{(k+1)} = \text{truncate}\left(\mathbf{Z}^{(k+1)} - \frac{\langle \mathbf{Q}^{(k)}, \mathbf{Z}^{(k+1)} \rangle}{\langle \mathbf{Q}^{(k)}, \mathbf{P}^{(k)} \rangle} \mathbf{P}^{(k)}\right)$
 - 11: $\mathbf{Q}^{(k+1)} = \text{truncate}(\mathbf{A}\mathbf{P}^{(k+1)})$
 - 12: $k = k + 1$
 - 13: **end while**
-

The PCG method in Algorithm 2 approximates the solution of a parameter-dependent linear system numerically within the hierarchical Tucker format if \mathbf{A} is positive definite and symmetric. In [13, Lemma 5] the authors proved that this algorithm converges if the truncation error ε is small enough. Algorithm 2 comprises additions and inner products of two tensors in hierarchical Tucker format which have an arithmetic cost in $\mathcal{O}(dnr^2 + dr^4)$, application of an operator which has an arithmetic cost in $\mathcal{O}(dn^2r)$, and evaluation of an entry of the represented tensor which has an arithmetic cost in $\mathcal{O}(dr^3)$. Hence, for small rank r most of the operations needed for the PCG method scale linearly in the dimension d and the mode size n , thus yielding an efficient method to solve parameter-dependent linear systems using low-rank tensor formats.

This means that, if we are able to prove the existence of a low-rank representation of the operator and right-hand side of the forward EMG problem, we can compute the solution of the linear system data-sparse and fast within the hierarchical Tucker format.

Finding conditions that guarantee the existence of a low-rank approximation for a given tensor is a research topic of its own [2, 4, 23]. This goes beyond the scope of this

article, and we thus assume that the solution of the parameter-dependent EMG forward problem has a low-rank approximation. This is backed up by the numerical experiments in Section 7.

4 The Bayes-inverse EMG problem

We present our first main contribution: The proof of the well-posedness of the Bayes-inverse EMG problem discussed in Section 2.

First we prove the existence of the posterior distribution ρ^{EMG} of T given measurements ϕ_{EMG}^{meas} for a prior ρ using the infinite-dimensional version of Bayes' theorem for inverse problems [5, Theorem 3.4].

Theorem 4.1 (Bayes' theorem for our inverse EMG problem). *Let Assumption 2.1 hold, and \mathbb{Q}_0 and \mathbb{Q}_T denote the measures with distribution $\mathcal{N}(0, \Xi)$ and $\mathcal{N}(\mathcal{G}_x(T), \Xi)$. Then,*

- B.1 *the scaling factor $Z := \int_{\mathcal{J}} \exp(-\Phi(T; \phi_{EMG}^{meas})) \rho(dT)$ is positive \mathbb{Q}_0 -almost surely,*
- B.2 *the potential $\Phi : \mathcal{J} \times \mathbb{R}^M \rightarrow \mathbb{R}$, as defined in (9), is ν_0 -measurable with product measure $\nu_0(dT, d\phi) := \rho(dT)\mathbb{Q}_0(d\phi)$,*
- B.3 *for ϕ_{EMG}^{meas} the conditional distribution ρ^{EMG} exists, ρ^{EMG} is absolutely continuous with respect to ρ , and*

$$\frac{d\rho^{EMG}}{d\rho}(T) = \frac{1}{Z} \exp(-\Phi(T; \phi_{EMG}^{meas}))$$

ν -almost surely with the product measure $\nu(dT, d\phi) := \rho(dT)\mathbb{Q}_T(d\phi)$.

To prove the above theorem, we need the boundedness and Lipschitz continuity of the observation operator as stated in the following lemma:

Lemma 4.2. *Let Assumption 2.1 hold. Then the observation operator is bounded and Lipschitz continuous with respect to T , i.e., there exist constants $0 < C, L_T < \infty$ such that*

$$\|\mathcal{G}_x(T)\|_{\mathbb{R}^M} \leq C \tag{12}$$

$$\left\| \mathcal{G}_x(T^1) - \mathcal{G}_x(T^2) \right\|_{\mathbb{R}^M} \leq L_T \left\| T^1 - T^2 \right\|_{\infty} \tag{13}$$

The proof consists of basic calculations and estimations on the weak form of the deterministic EMG forward problem and is thus left to the reader.

Proof of Theorem 4.1. The proof is based on the proof of the measurability of the potential Φ . Since B.1 and B.2 are the assumptions required for the Bayes Theorem in [5, Theorem 3.4] to hold, B.3 follows directly once B.1 and B.2 are proven. As the ν_0 -measurability of Φ , meaning that Φ is ρ -measurable in T and \mathbb{Q}_0 -measurable in ϕ_{EMG}^{meas} , follows from the Lipschitz continuity of the corresponding mappings, we show that

1. Φ is Lipschitz continuous with respect to T and
2. Φ is Lipschitz continuous with respect to $\phi_{\text{EMG}}^{\text{meas}}$.

Note that we also need the Lipschitz continuity of Φ to prove that the posterior depends continuously on the measurement data in Theorem 4.4. For ease of notations, we introduce the shorthand $\langle u, v \rangle_{\Xi} := \langle \Xi^{-\frac{1}{2}}u, \Xi^{-\frac{1}{2}}v \rangle$ for $u, v \in \mathbb{R}^M$ and neglect the second argument of the potential Φ .

1. Let $T_1, T_2 \in \mathcal{J}$ with $T_1 \neq T_2$, and (TI) and (HI) denote the triangle and Hölder's inequality. Using Lemma 4.2, we have

$$\begin{aligned}
& |\Phi(T_1) - \Phi(T_2)| \\
&= \frac{1}{2} |\langle \mathcal{G}(T_1), \mathcal{G}(T_1) \rangle_{\Xi} - \langle \mathcal{G}(T_2), \mathcal{G}(T_2) \rangle_{\Xi} + 2\langle \phi_{\text{EMG}}^{\text{meas}}, \mathcal{G}(T_2) - \mathcal{G}(T_1) \rangle_{\Xi}| \\
&\stackrel{\text{(TI)}}{\leq} \frac{1}{2} (\|\mathcal{G}(T_1)\|_{\Xi} \|\mathcal{G}(T_1) - \mathcal{G}(T_2)\|_{\Xi} + \|\mathcal{G}(T_1) - \mathcal{G}(T_2)\|_{\Xi} \|\mathcal{G}(T_2)\|_{\Xi}) \\
&\quad + \|\phi_{\text{EMG}}^{\text{meas}}\|_{\Xi} \|\mathcal{G}(T_2) - \mathcal{G}(T_1)\|_{\Xi} \\
&\stackrel{\text{(12)}}{\leq} C \|\mathcal{G}(T_2) - \mathcal{G}(T_1)\|_{\mathbb{R}^M} \stackrel{\text{(13)}}{\leq} CL_T \|T_1 - T_2\|_{\infty}.
\end{aligned}$$

2. For $\phi_1, \phi_2 \in \mathbb{R}^M$ with $\phi_1 \neq \phi_2$ we express the norms in the definition of Φ as scalar products obtaining

$$\begin{aligned}
|\Phi(T, \phi_1) - \Phi(T, \phi_2)| &= \frac{1}{2} \left| \|\phi_1 - \mathcal{G}(T)\|_{\Xi}^2 - \|\phi_1\|_{\Xi}^2 - \|\phi_2 - \mathcal{G}(T)\|_{\Xi}^2 + \|\phi_2\|_{\Xi}^2 \right| \\
&= |\langle (\phi_2 - \phi_1), \mathcal{G}(T) \rangle_{\Xi}| \stackrel{\text{(HI)}}{\leq} \|\phi_2 - \phi_1\|_{\Xi} \|\mathcal{G}(T)\|_{\Xi} \\
&\stackrel{\text{(12)}}{\leq} \underbrace{C \|\Xi\|_{\infty}^2}_{=: L_{\phi}} \|\phi_1 - \phi_2\|_{\mathbb{R}^M}. \tag{14}
\end{aligned}$$

This concludes the proof. \square

The well-posedness of the Bayes-inverse EMG problem also includes the continuity of the posterior ρ^{EMG} with respect to the data $\phi_{\text{EMG}}^{\text{meas}}$. Therefore, we need to define a metric on the space of measures. Similar to [5, 19] we choose the *Hellinger metric*.

Definition 4.3 (Hellinger metric). Let μ_1 and μ_2 denote two probability measures that are absolutely continuous with respect to a probability measure ζ . The *Hellinger metric* of μ_1 and μ_2 is then defined as

$$d_{\text{Hell}}(\mu_1, \mu_2) := \left(\frac{1}{2} \int \left(\sqrt{\frac{d\mu_1}{d\zeta}} - \sqrt{\frac{d\mu_2}{d\zeta}} \right)^2 d\zeta \right)^{\frac{1}{2}}.$$

With the help of the Hellinger metric we now prove the Lipschitz continuity of the posterior ρ^{EMG} with respect to measured EMG data.

Theorem 4.4. *Let Assumption 2.1 hold and let ρ^{EMG} denote the solution of our Bayes-inverse EMG problem given by Theorem 4.1. Then ρ^{EMG} depends Lipschitz continuously on the measured data ϕ_{EMG}^{meas} with respect to the Hellinger metric. This means there exists a positive constant $L > 0$ such that*

$$d_{\text{Hell}}(\rho_1^{EMG}, \rho_2^{EMG}) \leq L \|\phi_1 - \phi_2\|_{\Xi} \quad (15)$$

holds for all $\phi_1, \phi_2 \in \mathbb{R}^M$ and the posterior distributions ρ_1^{EMG} and ρ_2^{EMG} of σ_i given ϕ_1 and ϕ_2 .

To prove the above theorem, we need the following lemma:

Lemma 4.5. *Let Assumption 2.1 hold. Then $Z(\phi) = \int_{\mathcal{T}^3} \exp(-\Phi(T, \phi)) d\rho(T)$ is Lipschitz continuous in ϕ , i.e., there exists a constant $L_Z > 0$ such that*

$$|Z(\phi_1) - Z(\phi_2)| \leq L_Z \|\phi_1 - \phi_2\|_{\Xi} \quad (16)$$

holds for all $\phi_1, \phi_2 \in \mathbb{R}^M$ with $\phi_1 \neq \phi_2$.

The statement follows from Lemma 4.2 with basic calculations and estimations and is thus left to the reader.

Proof of Theorem 4.4. Let $\rho_1^{EMG}, \rho_2^{EMG}$ denote the solutions of the Bayes-inverse EMG problem for given measurements $\phi_1 \neq \phi_2$. For simplicity, we write $\Phi_j = \Phi(T, \phi_j)$ and $Z_j = Z(\phi_j)$, $j = 1, 2$. We estimate the Hellinger distance between the two posterior distributions using Young's inequality (YI), the Lipschitz continuity of the exponential function and the inverse of the square root on bounded domains with constants L_e and $L_{\text{sqr}}t$ and Lemma 4.5:

$$\begin{aligned} 2d_{\text{Hell}}(\rho_1^{EMG}, \rho_2^{EMG})^2 &= \int_{\mathcal{J}} \left[\left(\frac{1}{Z_1} \exp(-\Phi_1) \right)^{\frac{1}{2}} - \left(\frac{1}{Z_2} \exp(-\Phi_2) \right)^{\frac{1}{2}} \right]^2 d\rho(T) \\ &\stackrel{\text{(YI)}}{\leq} 2 \int_{\mathcal{J}} \frac{1}{Z_1} L_e^2 |\Phi_1 - \Phi_2|^2 d\rho(T) \\ &\quad \stackrel{\text{exp}, (\cdot)^{-\frac{1}{2}} \text{Lip.}}{\leq} 2 \int_{\mathcal{J}} L_{\text{sqr}}t^2 |Z_1 - Z_2|^2 \exp(-\Phi_2) d\rho(T) \\ &\stackrel{(16)}{\leq} 2 \int_{\mathcal{J}} \frac{1}{Z_1} L_e^2 L_{\phi}^2 \|\phi_1 - \phi_2\|_{\Xi}^2 d\rho(T) \\ &\quad + 2 \int_{\mathcal{J}} L_{\text{sqr}}t^2 L_Z^2 \|\phi_1 - \phi_2\|_{\Xi}^2 \exp(-\Phi_2) d\rho(T) \\ &= 2 \left(L_e^2 L_{\phi}^2 \frac{1}{Z_1} + L_{\text{sqr}}t^2 L_Z^2 Z_2 \right) \|\phi_1 - \phi_2\|_{\Xi}^2. \end{aligned}$$

As $Z_1 > 0$ holds, it follows that $\frac{1}{Z_1} < \infty$. It thus remains to prove that $Z_2 < \infty$ which is a consequence of \mathcal{G} being bounded and $\rho(\mathcal{J}) = 1$. The assertion follows with Lipschitz constant $L_{\rho}^2 := L_e^2 L_{\phi}^2 \frac{1}{Z_1} + L_{\text{sqr}}t^2 L_Z^2 Z_2$. \square

Remark 4.6. The estimate in (15) also describes the behavior of the posterior with respect to the discretization of the underlying equations and variables.

Recapitulating Theorems 4.1 and 4.4 shows that modeling the measurement error as a stochastic quantity leads to a regularization of our inverse EMG problem, see also [5].

5 Discretization and tensorization

While our goal is to solve the general Bayes-inverse EMG problem as described before, we verify our ansatz on a close-up of an arbitrary skeletal muscle.

We therefore assume from now on that $D = D_M$, i.e., there is no tissue surrounding the muscle tissue. Thus (4) vanishes from the problem description as well as the corresponding coupling and boundary conditions. We further assume that all muscle fibers are aligned parallel and belong to the same muscle, i.e., $\vec{d}_j = \vec{d}$, for all $j = 1, \dots, N_{MF}$, and a given muscle fiber direction $\vec{d} \in \mathbb{R}^3$. Lastly, we assume that the extracellular conductivity is a constant diagonal matrix, while the intracellular conductivity is diagonal but variable in space, i.e., $\vec{d} = \vec{e}_j$ with the canonical unit vectors $\vec{e}_j \in \mathbb{R}^3$, $j = 1, 2, 3$.

The resulting simplified forward problem is to find ϕ_e such that

$$\begin{aligned} \nabla \cdot ((\sigma_i + \sigma_e)\nabla\phi_e) &= -\nabla \cdot (\sigma_i\nabla V_m) && \text{in } D_M, \\ (\sigma_i\nabla V_m) \cdot \vec{n}_M &= -(\sigma_i\nabla\phi_e) \cdot \vec{n}_M && \text{on } \partial D_M, \\ (\sigma_e\nabla\phi_e) \cdot \vec{n}_M &= 0 && \text{on } \Gamma_M, \\ \int_{D_M} \phi_e &= 0, \end{aligned} \tag{17}$$

holds, with smoothed membrane potential $V_m = \sum_{j=1}^{N_{MF}} v_{m,j}(\pi_j(x)) \exp(-\frac{\beta}{2}\|x - \pi_j(x)\|^2)$ and one-dimensional muscle fiber membrane potential $v_{m,j}(s) = r_1 s^3 \exp(-r_2 s) - r_3$ for $s \in D_{F,j}$.

As mentioned in Section 2, we compute the posterior distribution ρ^{EMG} using the Metropolis-Hastings algorithm introduced in Algorithm 1. We obtain an approximation of the posterior by drawing a finite number of samples. Additionally, we discretize the forward operator \mathcal{G}_x as follows.

With $x = (x_1, x_2, x_3)^\top \in D_M$ the left-hand side of the first equation of (17) reads

$$A\phi_e := \nabla \cdot ((\sigma_i(x) + \sigma_e)\nabla\phi_e(x)) = \sum_{j=1}^3 \frac{\partial}{\partial x_j} \left((\sigma_i(x) + \sigma_e) \frac{\partial}{\partial x_j} \phi_e(x) \right) \tag{18}$$

and the right-hand side is given by

$$b := -\nabla \cdot (\sigma_i(x)\nabla V_m(x)) = \sum_{j=1}^3 -\frac{\partial}{\partial x_j} \left(\sigma_i(x) \frac{\partial}{\partial x_j} V_m(x) \right). \tag{19}$$

Since our forward solver uses a finite difference discretization, we consider the same discretization using centered differences of second order, and therefore assume that $\phi_e \in$

$C^4(D_M)$ and $\sigma_i \in C^1(D_M)$. This is reasonable under the assumption that $D = D_M$. Our theoretical and numerical results directly generalize to, e.g., finite element discretizations of arbitrary but given muscle geometries. The practical realization is future work.

In the following we use $h = (h_M, h_t, h_\sigma)$ to indicate the discretization of the muscle geometry by h_M , the time by h_t and the parameter space by h_σ . We denote the grid points by $(x_{j_1}, x_{j_2}, x_{j_3})$, $j_k = 0, \dots, n$, for $n \in \mathbb{N}$ and a discrete conductivity at grid point $(x_{j_1}, x_{j_2}, x_{j_3})$ by σ_{j_1, j_2, j_3} .

Theorem 5.1. *For*

$$B\phi := \nabla \cdot (\sigma(x)\nabla\phi(x)) = \sum_{j=1}^3 \frac{\partial}{\partial x_j} \left(\sigma(x) \frac{\partial}{\partial x_j} \phi(x) \right) \quad (20)$$

a second-order consistent stencil is given by

$$\begin{bmatrix} 0 & 0 & 0 \\ 0 & \frac{\sigma_{j,j,j-1} + \sigma_{j,j,j}}{2h_M^2} & 0 \\ 0 & 0 & 0 \end{bmatrix} \text{ in the first plane, in the second plane by}$$

$$\begin{bmatrix} 0 & \frac{\sigma_{j,j-1,j} + \sigma_{j,j,j}}{2h_M^2} & 0 \\ \frac{\sigma_{j-1,j,j} + \sigma_{j,j,j}}{2h_M^2} & -\frac{\sigma_{j-1,j,j} + \sigma_{j,j-1,j} + \sigma_{j,j,j-1} + 6\sigma_{j,j,j} + \sigma_{j,j,j+1} + \sigma_{j,j+1,j} + \sigma_{j+1,j,j}}{2h_M^2} & \frac{\sigma_{j,j,j} + \sigma_{j+1,j,j}}{2h_M^2} \\ 0 & \frac{\sigma_{j,j,j} + \sigma_{j,j+1,j}}{2h_M^2} & 0 \end{bmatrix}$$

and $\begin{bmatrix} 0 & 0 & 0 \\ 0 & \frac{\sigma_{j,j,j} + \sigma_{j,j,j+1}}{2h_M^2} & 0 \\ 0 & 0 & 0 \end{bmatrix}$ in the third plane.

Proof. Because of the Kronecker product structure of (20) the statement follows from the one-dimensional case. There, Taylor's theorem and equating the coefficients of

$$(B\phi)_j = (\sigma'(x_j)\phi'_j + \sigma(x_j)\phi''_j) \quad \text{and}$$

$$(B_h\phi_h)_j = \frac{1}{h_M^2} (-\tilde{\sigma}_j\phi_{j-1} + (\tilde{\sigma}_j + \tilde{\sigma}_{j+1})\phi_j - \tilde{\sigma}_{j+1}\phi_{j+1}),$$

yields $\tilde{\sigma}_j = \frac{\sigma_{j-1} + \sigma_j}{2}$ for a second-order consistent stencil given by

$$\frac{1}{h_M^2} \begin{bmatrix} \frac{\sigma_{j-1} + \sigma_j}{2} & -\frac{\sigma_{j-1} + 2\sigma_j + \sigma_{j+1}}{2} & \frac{\sigma_j + \sigma_{j+1}}{2} \end{bmatrix},$$

immediately finishing the proof. \square

Next, we derive an affine representation of the discrete operator and prove a low-rank tensor format representation of the operator and the right-hand side of the forward EMG problem. This is our second main contribution.

Corollary 5.2. *An affine representation of the discrete operator in the three-dimensional case is given by*

$$\begin{aligned} & \frac{\sigma_{j,j-1,j}}{h_M^2} M_{j,j-1,j} + \frac{\sigma_{j,j,j+1}}{h_M^2} M_{j,j,j+1} + \frac{\sigma_{j-1,j,j}}{h_M^2} M_{j-1,j,j} \\ & + \frac{\sigma_{j,j,j}}{h_M^2} M_{j,j,j} + \frac{\sigma_{j+1,j,j}}{h_M^2} M_{j+1,j,j} + \frac{\sigma_{j,j,j-1}}{h_M^2} M_{j,j,j-1} + \frac{\sigma_{j,j+1,j}}{h_M^2} M_{j,j+1,j}, \end{aligned}$$

where in the first plane the stencil is given by

$$\begin{aligned} M_{j,j-1,j}^{(:, :, 1)} &= M_{j,j,j+1}^{(:, :, 1)} = M_{j-1,j,j}^{(:, :, 1)} = M_{j,j,j}^{(:, :, 1)} = M_{j+1,j,j}^{(:, :, 1)} = \begin{bmatrix} 0 & 0 & 0 \\ 0 & 0 & 0 \\ 0 & 0 & 0 \end{bmatrix}, \\ M_{j,j,j-1}^{(:, :, 1)} &= \begin{bmatrix} 0 & 0 & 0 \\ 0 & \frac{1}{2} & 0 \\ 0 & 0 & 0 \end{bmatrix}, M_{j,j-1,j}^{(:, :, 1)} = \begin{bmatrix} 0 & 0 & 0 \\ 0 & 0 & 0 \\ 0 & 0 & 0 \end{bmatrix}, \end{aligned}$$

in the second plane by

$$\begin{aligned} M_{j,j-1,j}^{(:, :, 2)} &= \begin{bmatrix} 0 & \frac{1}{2} & 0 \\ 0 & -\frac{1}{2} & 0 \\ 0 & 0 & 0 \end{bmatrix}, M_{j,j,j+1}^{(:, :, 2)} = \begin{bmatrix} 0 & 0 & 0 \\ 0 & -\frac{1}{2} & 0 \\ 0 & 0 & 0 \end{bmatrix}, \\ M_{j-1,j,j}^{(:, :, 2)} &= \begin{bmatrix} 0 & 0 & 0 \\ \frac{1}{2} & -\frac{1}{2} & 0 \\ 0 & 0 & 0 \end{bmatrix}, M_{j,j,j}^{(:, :, 2)} = \begin{bmatrix} 0 & \frac{1}{2} & 0 \\ \frac{1}{2} & -3 & \frac{1}{2} \\ 0 & \frac{1}{2} & 0 \end{bmatrix}, \\ M_{j+1,j,j}^{(:, :, 2)} &= \begin{bmatrix} 0 & 0 & 0 \\ 0 & -\frac{1}{2} & \frac{1}{2} \\ 0 & 0 & 0 \end{bmatrix}, M_{j,j,j-1}^{(:, :, 2)} = \begin{bmatrix} 0 & 0 & 0 \\ 0 & -\frac{1}{2} & 0 \\ 0 & 0 & 0 \end{bmatrix}, M_{j,j-1,j}^{(:, :, 2)} = \begin{bmatrix} 0 & 0 & 0 \\ 0 & -\frac{1}{2} & 0 \\ 0 & \frac{1}{2} & 0 \end{bmatrix}, \end{aligned}$$

and in the third plane by

$$\begin{aligned} M_{j,j-1,j}^{(:, :, 3)} &= \begin{bmatrix} 0 & 0 & 0 \\ 0 & 0 & 0 \\ 0 & 0 & 0 \end{bmatrix}, M_{j,j,j+1}^{(:, :, 3)} = \begin{bmatrix} 0 & 0 & 0 \\ 0 & \frac{1}{2} & 0 \\ 0 & 0 & 0 \end{bmatrix}, \\ M_{j-1,j,j}^{(:, :, 3)} &= M_{j,j,j}^{(:, :, 3)} = M_{j+1,j,j}^{(:, :, 3)} = M_{j,j,j-1}^{(:, :, 3)} = M_{j,j-1,j}^{(:, :, 3)} = \begin{bmatrix} 0 & 0 & 0 \\ 0 & 0 & 0 \\ 0 & 0 & 0 \end{bmatrix}. \end{aligned}$$

Proof. Follows from Theorem 5.1 with linearity. \square

We define $A_h^{(0)} := A_{h,\sigma_e}$ denoting the discrete operator given by Theorem 5.1 for constant $\sigma_e \in \mathbb{R}^{3 \times 3}$ and A_{h,j_1,j_2,j_3} denoting the discrete operator given by the stencil M_{j_1,j_2,j_3} from Corollary 5.2. Then the discrete operator of (18) is given by

$$A_h := A_{h,\sigma_e} + \sum_{j_1=1}^{m_1} \sum_{j_2=1}^{m_2} \sum_{j_3=1}^{m_3} \sigma_{j_1,j_2,j_3} A_{h,j_1,j_2,j_3}.$$

Using the vectorizations $\text{vec}(A_{h,j_1,j_2,j_3}) =: A_h^{(k)}$ and $\text{vec}(\sigma_{j_1,j_2,j_3}) =: p^{(k)}$, see Definition 3.3, yields a parameter-dependent affine structure of the form

$$A_h(p) := A_h^{(0)} + \sum_{k=1}^d p^{(k)} A_h^{(k)}$$

with $p := (p^{(1)}, \dots, p^{(d)})$, where each $A_h^{(k)}$ is constant, i.e., $A_h^{(k)}$ is parameter-independent. Note that in general the conductivity can be an arbitrary matrix, while we only consider diagonal conductivities σ_i here for reasons of simplicity. If we further assume that σ_i is constant, we obtain three different parameters, namely the diagonal entries of σ_i .

We now take a closer look at the right-hand side and discretize the time variable t in (1) using equidistant time steps $t_j = jh_t$, $j = 0, \dots, t_{\max}$ for time step size h_t . Multiplying this with the AP velocities u_k , $k = 1, \dots, N_{\text{MF}}$, we achieve $s_j = u_k t_j$ for the discretization of the muscle fiber coordinate s .

Furthermore, we remark that the linear dependency of the right-hand side on the intracellular conductivity is obvious under our assumptions, which include that the muscle fiber direction is one of the standard unit vectors, i.e., $\vec{d} = \vec{e}_j$, $j \in \{1, 2, 3\}$. If V_m is independent of σ_i , the structure of the right-hand side is the same as the structure of the operator. Then we see the linear structure of (19) that has the form

$$b_h(p) := \sum_{k=1}^d p^{(k)} b_h^{(k)}.$$

How to represent an arbitrary right-hand side in a parameter-dependent way is ongoing research.

We now discretize the parameter space by choosing a finite number of parameters $p_h := (p_h^{(1)}, \dots, p_h^{(\ell)}, \dots, p_h^{(d)})$ from a discrete set \mathcal{I} . We fix discrete values for all $p_h^{(\ell)}$, i.e., $p_h^{(\ell)} \in \{p_h^{(\ell)}(1), p_h^{(\ell)}(2), \dots, p_h^{(\ell)}(n_\ell)\} =: \mathcal{I}_\ell$, and reformulate our problem as:

$$\text{Solve } A_h(p_h)\phi_h(p_h, t) = b_h(p_h, t) \text{ for all } p_h \in \mathcal{I}. \quad (21)$$

Applying classical methods one has to solve a system of $\prod_{\ell=1}^d n_\ell \approx n^d$ linear equations. To overcome the curse of dimensionality in this case, we exploit the structure of the linear system, see Section 3. We find a data-sparse representation of the problem that allows us to solve the parameter-dependent system for all $p_h \in \mathcal{I}$ simultaneously, analogously to [11]. For computing the solution of (21) for all possible $p_h \in \mathcal{I}$, we define a large block-diagonal system with the operator

$$\mathbf{A} := \begin{pmatrix} A_1^{(0)} & 0 & \dots & 0 \\ 0 & A_2^{(0)} & \ddots & \vdots \\ \vdots & \ddots & \ddots & 0 \\ 0 & \dots & 0 & A_n^{(0)} \end{pmatrix} =: \text{blkdiag}(A_1^{(0)}, \dots, A_n^{(0)}),$$

where $A_j^{(0)} = A_h^{(0)} + \sum_{\ell=1}^d p_h^{(\ell)}(j) A_h^{(\ell)}$ denotes the j -th diagonal block.

The memory requirement to store \mathbf{A} , however, grows exponentially in n and thus, even for moderate values of d and n_ℓ , a classical representation of our problem is infeasible. Therefore, we reformulate the problem using the notation $A_j^{(m)} = \sum_{\ell=m}^d p_h^{(\ell)}(j) A_h^{(\ell)}$, $m = 1, \dots, d$, and Id_{n_k} denoting the identity in $\mathbb{R}^{n_k \times n_k}$, and achieve:

$$\begin{aligned}
\mathbf{A} &= \text{blkdiag} \left(A_h^{(0)} + A_1^{(1)}, A_h^{(0)} + A_2^{(1)}, \dots, A_h^{(0)} + A_n^{(1)} \right) \\
&= \text{blkdiag} \left(A_h^{(0)}, A_h^{(0)}, \dots, A_h^{(0)} \right) \\
&\quad + \text{blkdiag} \left(p_h^{(1)}(1) A_h^{(1)}, p_h^{(1)}(2) A_h^{(1)}, \dots, p_h^{(1)}(n_1) A_h^{(1)} \right) \\
&\quad + \text{blkdiag} \left(A_1^{(2)}, A_2^{(2)}, \dots, A_n^{(2)} \right) \\
&= \text{Id}_{n_d} \otimes \dots \otimes \text{Id}_{n_2} \otimes \text{Id}_{n_1} \otimes A^{(0)} \\
&\quad + \text{Id}_{n_d} \otimes \dots \otimes \text{Id}_{n_2} \otimes \text{diag} \left(p_h^{(1)} \right) \otimes A_h^{(1)} \\
&\quad + \dots + \text{diag} \left(p_h^{(d)} \right) \otimes \dots \otimes \text{Id}_{n_2} \otimes \text{Id}_{n_1} \otimes A_h^{(d)}.
\end{aligned}$$

This leads to the following data-sparse CP representation of the operator

$$\mathbf{A} = \sum_{k=0}^d \bigotimes_{\ell=0}^d A_h^{(k)}(\ell) \quad \text{where } A_h^{(k)}(\ell) = \begin{cases} A_h^{(\ell)} & \text{if } \ell = d, \\ \text{diag} \left(p_h^{(\ell)} \right) & \text{if } \ell + k = d \text{ and } k \neq 0, \\ \text{Id}_{n_{d-k}} & \text{otherwise} \end{cases}$$

with discrete parameters $p_h^{(\ell)} = (p_h^{(\ell)}(1), \dots, p_h^{(\ell)}(n_\ell)) \in \mathcal{I}_\ell$. Similar results can be obtained for the right-hand side.

Concluding, we represent the operator and the right-hand side of (21) exactly using low-rank tensor formats. Further, we approximate the solution of (21) using the hierarchical Tucker format in Algorithm 2.

6 The tensorized Metropolis-Hastings algorithm

Having proved the theory for our Bayes-inverse EMG problem and a low-rank tensor representation of the operator and right-hand side of the discrete forward EMG problem, we now derive our final main contribution: A fast tensorized Metropolis-Hastings algorithm. Therefore, we combine the precomputation of the forward EMG problem for all parameters simultaneously using the hierarchical Tucker format and Algorithm 2 with the Metropolis-Hastings sampling, see Algorithm 1.

To be more precise, we first choose a fixed number of samples $J \in \mathbb{N}$ that have to be drawn during the sampling process, i.e., the sampling loop runs for $j = 1, \dots, J$. Before entering the sampling loop in line 1 of Algorithm 1, we precompute the solution of the parameter-dependent forward EMG problem in the hierarchical Tucker format using the PCG method from Algorithm 2 and store the data-sparse solution. Recall that storing the solution of the parameter-dependent problem for all parameters is only feasible within data-sparse formats like the hierarchical Tucker format.

We now enter the sampling loop of Algorithm 1. Note that we directly sample the diagonal entries of the conductivity tensor σ_i instead of the coefficients $(T_j)_{j \geq 1}$ as we assume σ_i to be constant. Further, instead of solving the discretized forward EMG problem in line 4, we evaluate the precomputed tensor solution with arithmetic cost in $\mathcal{O}(ndr^3)$.

We assume that the cost of drawing one sample from the posterior distribution equals the solution time T_s of the discretized forward EMG problem for the standard Metropolis-Hastings algorithm and the evaluation time T_e of the precomputed tensor solution for the tensorized Metropolis-Hastings algorithm. Thus, the runtime of the standard Metropolis-Hastings algorithm is JT_s , while the runtime of the tensorized algorithm is the sum of the precomputation time T_p and the evaluation times, i.e., $T_p + JT_e$. We notice that asymptotically the speedup $\frac{JT_s}{T_p + JT_e}$ is limited by $\frac{T_s}{T_e}$ for $J \rightarrow \infty$.

Based on our mathematical theory we expect that the Markov chains constructed by both algorithms behave similarly. This is due to the fact that we exactly represent the operator and the right-hand side of the forward EMG problem for all discrete parameter combinations within the hierarchical Tucker format. Additionally, we compute the tensor solution using Algorithm 2 with specified truncation accuracy, resulting in an error-controlled approximation.

7 Numerical experiments

We illustrate our method for the inverse EMG problem with numerical experiments. We conduct all experiments in MATLAB using the KerMor framework¹ and the `htucker` toolbox [21]. Throughout our experiments we use the following default settings.

The geometry that we use is a muscle cuboid of size 4 cm \times 2 cm \times 1 cm that is equipped with 30 \times 30 muscle fibers. The muscle geometry is discretized using the grid size $h_M = \frac{1}{3}$ while the muscle fibers are discretized using 30 grid points, and we use 101 time steps. We fix the extracellular conductivity at $\sigma_e = \text{diag}(6.7, 6.7, 6.7)$. As reference conductivity we choose $\sigma_i^{\text{ref}} = \text{diag}(0.893, 8.930, 0.893)$, i.e., the muscle fiber direction is the second unit vector and the muscle fibers are aligned parallel to the second coordinate axis. We allow the muscle fiber direction to be one of the three unit vectors. As upper bound on the conductivity we define $s_+ = 10$ and $s_- = 0.001$ as lower bound which we also set as the discretization step size in the parameter space, i.e., $h_\sigma = s_-$.

For computing the tensor solution of (21), we use Algorithm 2. There we set $k_{\max} = 15$, $\varepsilon = 1 \times 10^{-4}$ and we truncate to a relative accuracy of 1×10^{-6} . As preconditioner we define $\mathbf{M} := \text{Id}_{n_d} \otimes \dots \otimes \text{Id}_{n_1} \otimes A_h^{(0)}$ which proved reasonable in former experiment runs. We compute the tensor solution on a suitable conductivity grid with grid size h_σ and $A_h^{(0)}$ using the conductivity at the midpoint of that grid. For handling the time-dependency in the right-hand side, we solve the corresponding linear system for all time steps simultaneously. This leads to a tensor of size 364 \times 101 \times 4000 \times 4001 \times 4000.

For sampling from the posterior distribution of intracellular conductivity given EMG measurements, we use Algorithm 1. There we set the total number of samples to 500 000

¹<https://www.morepas.org/software/kermor/index.html>

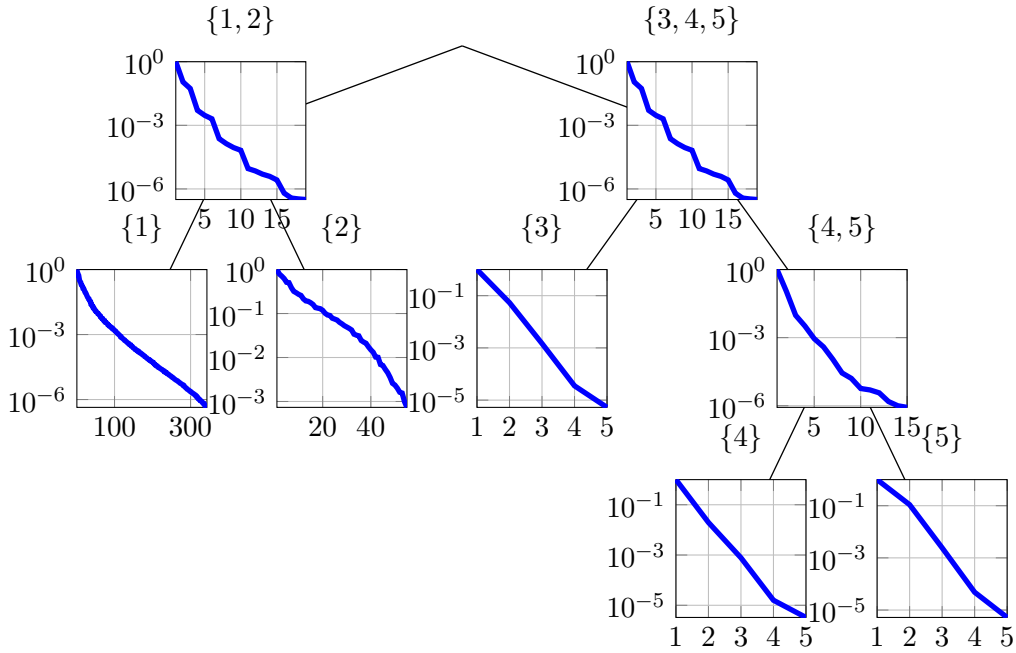


Figure 3: Relative singular values of the corresponding matricization of the low-rank solution of the forward EMG problem.

and use Gaussian noise with $\xi = 2.0$. The algorithm draws a conductivity proposal in a sampling radius $\delta = 1.5$ around the last accepted sample. As default we draw the initial guess from a uniform distribution on an interval with radius δ around the reference solution, and we discard the first 200 samples as burn-in. These choices proved reasonable in our parameter studies. Additionally, we modify the algorithm such that it also samples the muscle fiber direction as one of the unit vectors.

We call Algorithm 1 using the MATLAB build-in QR decomposition to solve the forward problem for the proposed conductivity in each iteration the *standard algorithm* (SA), and we call Algorithm 1 using the precomputed tensor solution the *tensorized algorithm* (TA).

Rank of the hierarchical Tucker format solution

In our first numerical experiment, we examine the hierarchical Tucker rank, see Definition 3.4, of the tensor solution of the linear system to support our assumption that the solution is well approximated with low rank. Further, a small rank is important for efficient arithmetic operations as some of these operations in low-rank tensor formats scale in $\mathcal{O}(r^4)$, see Section 3. Therefore, in Figure 3 we show a logarithmic-linear plot of the relative singular values for the corresponding matricizations of the solution of the forward problem using our default setting. We observe that the rank of the matricization remains smaller than 6 in the parameter space, i.e., the rank of the matricizations corresponding to $\{3\}$, $\{4\}$, and $\{5\}$. We also see that the rank of the matricization corre-

Table 1: Comparison of the standard algorithm (SA) and the tensorized algorithm (TA) with 500 000 drawn samples, Gaussian noise with $\xi = 2.0$, and sampling radius $\delta = 1.5$.

	$\sigma_{i,\text{ref}}^1$		$\sigma_{i,\text{ref}}^2$	
	SA	TA	SA	TA
Acceptance rate (%)	5.39	5.38	5.79	5.79
MAD($\sigma_{i,11}$)	0.86	0.86	0.50	0.50
MAD($\sigma_{i,22}$)	0.44	0.44	0.24	0.24
MAD($\sigma_{i,33}$)	0.17	0.17	0.55	0.55
Var($\sigma_{i,11}$)	1.05	1.05	0.38	0.38
Var($\sigma_{i,22}$)	0.29	0.29	0.09	0.09
Var($\sigma_{i,33}$)	0.04	0.04	0.44	0.44

sponding to $\{2\}$ is 55 while the rank of the matricization corresponding to $\{1\}$ is 343. We expect that the matricization corresponding to $\{1\}$ has full rank since this separates the spatial dimension, i.e., $\{1\}$, and the time dimension, i.e., $\{2\}$, and since each time step yields its own right-hand side. Using tensor formats, we reduce the theoretical storage cost of the full tensor from 1.88×10^{10} MB ($\approx 18\,800\,000$ GB) to 4.41 MB counting the storage cost for 1 entry as 64 bit.

Comparison of the tensorized algorithm and the standard algorithm

For the validation of our tensorized algorithm, we compare its statistical behavior to the standard Metropolis-Hastings algorithm. We run both algorithms in our default setting for the reference conductivities $\sigma_{i,\text{ref}}^1 = \text{diag}(0.893, 8.930, 0.893)$ and $\sigma_{i,\text{ref}}^2 = \text{diag}(0.893, 0.893, 8.930)$.

We present the acceptance rates $\frac{\#\text{samples acc.}}{\#\text{samples drawn}}$, the mean absolute deviations (MADs) $\frac{1}{\#\text{samples acc.}} \sum_{k=1}^{\#\text{samples acc.}} |\sigma_i^{(k)} - \bar{\sigma}_i|$ and variance $\frac{1}{\#\text{samples acc.} - 1} \sum_{k=1}^{\#\text{samples acc.}} (\sigma_i^{(k)} - \bar{\sigma}_i)^2$ of the accepted diagonal entries of the conductivities in Table 1. For the reference values $\sigma_{i,\text{ref}}^1$ and $\sigma_{i,\text{ref}}^2$ we observe that both methods have similar acceptance rates. We further notice that the SA and TA have a comparable reliability, i.e., comparable MAD and variance.

We conclude that the sampling process of both algorithms is similar and that our tensor approach is therefore a promising ansatz to accelerate the SA if the discretization error of the forward problem is small. In this case, we furthermore reason that our results indicate that the tensor solution of the forward EMG problem is indeed a good approximation to the solution that we obtain using the MATLAB build-in QR decomposition. We highlight that these results are in line with our theoretical findings from Section 5.

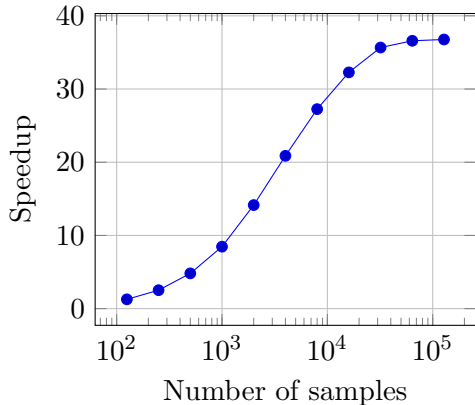


Figure 4: Speedup of the tensorized algorithm compared to the standard algorithm for fixed grid size and a varying number of samples.

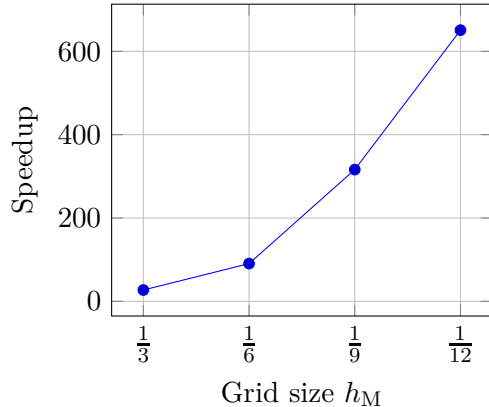


Figure 5: Estimated speedup of the tensorized algorithm compared to the standard algorithm for varying grid size h_M and 100 000 samples.

Speedup tests

First, we examine the speedup $\frac{\text{runtime SA}}{\text{runtime TA}}$ of our tensor method compared to the standard method for fixed discretization grid size h_M and varying number of samples. Therefore, we run both algorithms in the default setting for 125 samples and double the number of samples until we reach 128 000 samples. We present the speedup of the TA compared to the SA in Figure 4.

We observe that the speedup curve grows steadily and flattens as the number of samples increases. This is due to the fact that the influence of the precomputation time of the TA, which is $\bar{T}_p \approx 13.71$ s on average, decreases with growing number of samples. As mentioned in Section 6, the speedup is bounded by the quotient $\frac{\bar{T}_s}{\bar{T}_e}$. We insert the average time $\bar{T}_s \approx 0.1481$ s needed for one sample using the SA and the average time $\bar{T}_e \approx 0.0037$ s needed for one sample using the TA and obtain an upper bound of 39.60 for the speedup. For 128 000 samples the speedup is 36.77, which corresponds to a runtime of 5.27 h using the SA, compared to 0.14 h (≈ 8.59 min) using the TA.

Further, we run both algorithms in the default setting for grid sizes $h_M = \frac{1}{3}, \frac{1}{6}, \frac{1}{9}, \frac{1}{12}$. Furthermore, to reduce the overall computation time, we reduce the number of samples to 100. We use our findings from Section 6 to extrapolate the measured sampling times to 100 000 samples. To be more precise, we first compute the average time for drawing one sample with both algorithms, then scale this number by 100 000 to achieve estimates on T_e for the TA and T_s for the SA and add the measured precomputation time T_p for the TA. Note that the precomputation time is independent of the number of samples. Figure 5 shows the speedup resulting from this extrapolation.

As expected, we observe that the speedup in Figure 5 grows steadily and is unbounded in contrast to the speedup for fixed grid size and increasing number of samples. For

$h_M = \frac{1}{12}$ we observe a speedup of 650.81 which corresponds to a runtime of 2.87 h for the TA compared to a runtime of 1864.91 h (≈ 77.70 d) for the SA.

We expect that the TA outperforms the SA for realistic muscle geometries or fine grid sizes. Furthermore, we conclude that using the TA enables us to solve problems that are infeasible to solve using the SA, in reasonable time.

8 Related work

To overcome the ill-posedness of inverse problems, regularization methods like the Tikhonov regularization are a widely used ansatz, see, e.g., [8] and the references therein. The Tikhonov regularization was used in [9, 31] to reconstruct the electrical conductivity of biological tissue from EMG measurements. Moreover, in [31] model order reduction was used to accelerate the computations. A difference to our approach is that regularization methods neglect the inevitable measurement error.

For other Bayes-inverse problems different approaches to speedup the sampling process have been examined, e.g., in [19] the authors used a method based on polynomial chaos expansions to construct a surrogate of the forward problem. In [28] quasi Monte Carlo methods and multilevel Monte Carlo methods were used to accelerate the convergence of the sampling algorithm.

Furthermore, low-rank tensor methods were examined in the context of Bayes-inverse problems. In [6] low-rank tensor formats were used to compute a surrogate of the target distribution. There the authors directly approximated the target distribution using a generalization of the cross approximation. In [7] the authors used low-rank tensor formats to approximate the stochastic Galerkin solution of the parameter-dependent forward problem to achieve a discrete representation of the posterior distribution.

9 Conclusion

Applying mathematical theory results in an efficient algorithm to solve the Bayes-inverse EMG problem. Proving the well-posedness of the Bayes-inverse EMG problem guarantees the convergence of this algorithm. Further, proving a data-sparse representation of the forward EMG problem allows for the efficient precomputation of the parameter-dependent forward solution. The presented numerical experiments support this mathematical theory but also indicate that a high number of samples is required to obtain accurate results. The sampling algorithm which uses the data-sparse representation of the forward EMG problem computes this high number of samples in a reasonable time.

The mathematical theory of the Bayes-inverse problem holds for general symmetric positive definite conductivities and thus for arbitrary muscle fiber directions. The low-rank representation of the forward EMG problem, however, holds for fixed muscle fiber directions only. In our numerical experiments the speedup using tensor methods enables solving problems with grid sizes that are infeasible using classical methods. Therefore, future work is the generalization of the low-rank representation of the right-hand side of the forward EMG problem to arbitrary muscle fiber directions. This generalization

could enable the computation of realistic problems in medical applications and lead to a non-invasive and radiation-free imaging method.

Acknowledgments

We thank Maren Klever for her critical reading of and suggestions for this article.

This research was partially funded by the Deutsche Forschungsgemeinschaft (DFG, German Research Foundation) under Germany's Excellence Strategy – EXC-2075 – 390740016.

L. Grasedyck and T. A. Werthmann have been supported by the DFG within the DFG priority program 1886 (SPPPoly) under Grant No. GR-3179/5-1.

References

- [1] A. Alexanderian. “A brief note on the Karhunen-Loève expansion”. In: *arXiv e-prints*, arXiv:1509.07526 (2015). arXiv: 1509.07526 [math.PR].
- [2] M. Bachmayr and R. Schneider. “Iterative Methods Based on Soft Thresholding of Hierarchical Tensors”. In: *Foundations of Computational Mathematics* 17.4 (2017), pp. 1037–1083. DOI: 10.1007/s10208-016-9314-z.
- [3] J. D. Carroll and J.-J. Chang. “Analysis of individual differences in multidimensional scaling via an n-way generalization of “Eckart-Young” decomposition”. In: *Psychometrika* 35.3 (1970), pp. 283–319. DOI: 10.1007/BF02310791.
- [4] W. Dahmen, R. DeVore, L. Grasedyck, and E. Süli. “Tensor-Sparsity of Solutions to High-Dimensional Elliptic Partial Differential Equations”. In: *Foundations of Computational Mathematics* 16.4 (2016), pp. 813–874. DOI: 10.1007/s10208-015-9265-9.
- [5] M. Dashti and A. M. Stuart. “The Bayesian Approach to Inverse Problems”. In: *Handbook of Uncertainty Quantification*. Ed. by R. Ghanem, D. Higdon, and H. Owhadi. Cham: Springer International Publishing, 2017, pp. 311–428. DOI: 10.1007/978-3-319-12385-1_7.
- [6] S. Dolgov, K. Anaya-Izquierdo, C. Fox, and R. Scheichl. “Approximation and sampling of multivariate probability distributions in the tensor train decomposition”. In: *Statistics and Computing* 30.3 (2020), pp. 603–625. DOI: 10.1007/s11222-019-09910-z.
- [7] M. Eigel, M. Marschall, and R. Schneider. “Sampling-free Bayesian inversion with adaptive hierarchical tensor representations”. In: *Inverse Problems* 34.3 (2018), p. 035010. DOI: 10.1088/1361-6420/aaa998.
- [8] H. W. Engl, M. Hanke, and A. Neubauer. *Regularization of Inverse Problems*. Vol. 375. Springer series in mathematics and its applications. Springer Netherlands, 2000, pp. VIII, 321.

- [9] L. S. Graham and D. Kilpatrick. “Estimation of the Bidomain Conductivity Parameters of Cardiac Tissue From Extracellular Potential Distributions Initiated by Point Stimulation”. In: *Annals of Biomedical Engineering* 38.12 (2010), pp. 3630–3648. DOI: 10.1007/s10439-010-0119-y.
- [10] L. Grasedyck. “Hierarchical Singular Value Decomposition of Tensors”. In: *SIAM Journal on Matrix Analysis and Applications* 31.4 (2010), pp. 2029–2054. DOI: 10.1137/090764189.
- [11] L. Grasedyck, M. Klever, C. Löbber, and T. A. Werthmann. “A parameter-dependent smoother for the multigrid method”. In: *Computing and Visualization in Science* (2019). Forthcoming.
- [12] L. Grasedyck, D. Kressner, and C. Tobler. “A literature survey of low-rank tensor approximation techniques”. In: *GAMM-Mitteilungen* 36.1 (2013), pp. 53–78. DOI: 10.1002/gamm.201310004.
- [13] L. Grasedyck and C. Löbber. “Distributed hierarchical SVD in the Hierarchical Tucker format”. In: *Numerical Linear Algebra with Applications* 25.6 (2018), e2174. DOI: 10.1002/nla.2174.
- [14] W. Hackbusch. *Tensor Spaces and Numerical Tensor Calculus*. Vol. 42. Springer series in computational mathematics. Heidelberg: Springer, 2012, pp. xxiv, 500. DOI: 10.1007/978-3-642-28027-6.
- [15] W. Hackbusch, B. N. Khoromskij, and E. E. Tyrtyshnikov. “Approximate iterations for structured matrices”. In: *Numerische Mathematik* 109.3 (2008), pp. 365–383. DOI: 10.1007/s00211-008-0143-0.
- [16] W. Hackbusch and S. Kühn. “A New Scheme for the Tensor Representation”. In: *Journal of Fourier Analysis and Applications* 15.5 (2009), pp. 706–722. DOI: 10.1007/s00041-009-9094-9.
- [17] J. Hadamard. “Sur les problèmes aux dérivées partielles et leurs signification physique”. In: *Princeton University Bulletin* 13.4 (1902), pp. 49–52.
- [18] R. Harshman. “Foundations of the PARAFAC procedure: Models and conditions for an "explanatory" multi-model factor analysis”. In: *UCLA Working Papers in Phonetics*. 1970, pp. 1–84.
- [19] V. H. Hoang, C. Schwab, and A. M. Stuart. “Complexity analysis of accelerated MCMC methods for Bayesian inversion”. In: *Inverse Problems* 29.8 (2013), p. 085010. DOI: 10.1088/0266-5611/29/8/085010.
- [20] P. R. Johnston. “A sensitivity study of conductivity values in the passive bidomain equation”. In: *Mathematical Biosciences* 232.2 (2011), pp. 142–150. DOI: 10.1016/j.mbs.2011.05.004.
- [21] D. Kressner and C. Tobler. “Algorithm 941: htucker—A Matlab Toolbox for Tensors in Hierarchical Tucker Format”. In: *ACM Transactions on Mathematical Software* 40.3 (2014), pp. 1–22. DOI: 10.1145/2538688.

- [22] D. Kressner and C. Tobler. “Low-Rank Tensor Krylov Subspace Methods for Parametrized Linear Systems”. In: *SIAM Journal on Matrix Analysis and Applications* 32.4 (2011), pp. 1288–1316. DOI: 10.1137/100799010.
- [23] D. Kressner and A. Uschmajew. “On low-rank approximability of solutions to high-dimensional operator equations and eigenvalue problems”. In: *Linear Algebra and its Applications* 493 (2016), pp. 556–572. DOI: 10.1016/j.laa.2015.12.016.
- [24] K. S. Miller. “On the Inverse of the Sum of Matrices”. In: *Mathematics Magazine* 54.2 (1981), pp. 67–72. DOI: 10.2307/2690437.
- [25] M. Mordhorst, T. Heidlauf, and O. Röhrle. “Predicting electromyographic signals under realistic conditions using a multiscale chemo–electro–mechanical finite element model”. In: *Interface Focus* 5.2 (2015), p. 20140076. DOI: 10.1098/rsfs.2014.0076.
- [26] J. R. Norris. *Markov Chains*. Cambridge Series in Statistical and Probabilistic Mathematics. Cambridge University Press, 1997. DOI: 10.1017/CB09780511810633.
- [27] P. Rosenfalck. “Intra-and extracellular potential fields of active nerve and muscle fibres: A physico-mathematical analysis of different models”. In: *Acta Physiologica Scandinavica. Supplementum* 321 (1969), pp. 1–168.
- [28] R. Scheichl, A. M. Stuart, and A. L. Teckentrup. “Quasi-Monte Carlo and Multi-level Monte Carlo Methods for Computing Posterior Expectations in Elliptic Inverse Problems”. In: *SIAM/ASA Journal on Uncertainty Quantification* 5.1 (2017), pp. 493–518. DOI: 10.1137/16M1061692.
- [29] V. de Silva and L.-H. Lim. “Tensor Rank and the Ill-Posedness of the Best Low-Rank Approximation Problem”. In: *SIAM Journal on Matrix Analysis and Applications* 30.3 (2008), pp. 1084–1127. DOI: 10.1137/06066518X.
- [30] A. M. Stuart. “Inverse problems: A Bayesian perspective”. In: *Acta Numerica* 19 (2010), pp. 451–559. DOI: 10.1017/S0962492910000061.
- [31] H. Yang and A. Veneziani. “Efficient estimation of cardiac conductivities via POD-DEIM model order reduction”. In: *Applied Numerical Mathematics* 115 (2017), pp. 180–199. DOI: 10.1016/j.apnum.2017.01.006.